PAPER

Check for updates

Imine bond-directed assembly of polyoxometalate-based metal–organic frameworks†

Xiang Yu,‡ Xinyu Xu,‡ Lei Gao, Rengan Luo, Yi-Fan Liu, Yu-Hao Gu [ID] and Shuai Yuan [ID] *

Polyoxometalate-based metal–organic frameworks (POMOFs) are highly effective heterogeneous catalysts that combine the catalytic activity of polyoxometalates (POMs) with the high surface area, tunable porosity, and structural diversity of MOFs. Nevertheless, there is still a lack of a general method to integrate POMs with various transition metal-based building units into POMOFs under mild conditions. In this work, we employed imine bonds to link amino-functionalized Anderson-type POMs with aldehyde-terminated divalent metal clusters, resulting in a series of isostructural POMOFs, M(II)-POMOFs (M = Zn, Co, Mg, or Mn). Furthermore, we used post-synthetic metal exchange and oxidation to transform Zn-POMOF into Fe(III)-POMOF with strong Lewis acidic Fe^{3+} sites. Notably, both the synthesis and post-synthetic modifications were performed under mild conditions (room temperature, acid-free), preventing the decomposition of the POMs. Compared to M(II)-POMOFs or MOFs without POMs, the combination of Lewis acidic Fe^{3+} and POMs enhanced its catalytic activity for CO_2 cycloaddition with epoxides, enabling efficient synthesis of cyclic carbonates. This versatile synthetic method could broaden the scope of POMOFs, extending their applications in catalysis and beyond.

Introduction

Polyoxometalates (POMs) are known for their rich redox chemistry, strong Brønsted/Lewis acidity, and ability to mediate complex multielectron processes, making them highly effective catalysts.[1–3] By incorporating POMs into metal–organic frameworks (MOFs), polyoxometalate-based metal–organic frameworks (POMOFs) combine the structural characteristics of MOFs with the functionality of POMs.[4–7] These materials possess high surface areas, tunable porosities, and the ability to design specific functionalities.[8] Therefore, POMOFs have shown wide-ranging applications in catalysis, energy storage, photochemistry, medicine, and environmental remediation.[9] POMOFs have been intensively studied as heterogeneous catalysts in a wide range of applications, including oxidation reactions, photocatalysis, and acid-catalyzed processes.[10–13] For example, POMOFs are effective catalysts for oxidative transformations, such as the selective oxidation of alcohols to aldehydes or ketones, which is vital in fine chemical production.[14,15] They also play crucial roles in photocatalytic processes, including water splitting and CO_2 reduction, where the photoactive POM units facilitate light absorption and electron transfer.[16–18] An example of the acid-catalyzed process is the CO_2 cycloaddition reaction with epoxides to form cyclic carbonates, where POMOFs act as Lewis acidic sites.[19] For example, Lan *et al.* synthesized two novel POMOFs based on polyoxovanadates with Lewis acid sites, which showed good catalytic activity and high selectivity in the CO_2 cycloaddition reaction.[20]

Conventional synthetic POMOFs can be primarily categorized into three types: (i) POMs serve as inorganic secondary building units (SBUs, Scheme 1a);[21] (ii) POMs act as guest molecules encapsulated *in situ* in MOFs (POM@MOFs, Scheme 1b);[22] and (iii) POMs act as linkers, coordinating with metals through self-assembly to form POMOFs (Scheme 1c).[23] These methods have been successfully applied to synthesize diverse POMOFs with various structures and functions. However, most of these methods are restricted to the synthesis of low-valent metal-based MOFs. This is due to the harsh synthetic conditions (*i.e.* high temperature, acids as modulators) of high-valent metal-based MOFs, which are incompatible with the stability window of certain POMs.[24,25] In addition, the products of methods (i) and (ii) can be difficult to control in the

*State Key Laboratory of Coordination Chemistry, School of Chemistry and Chemical Engineering, Nanjing University, Nanjing 210023, China.
E-mail: syuan@nju.edu.cn*

‡These authors contributed equally to this work.
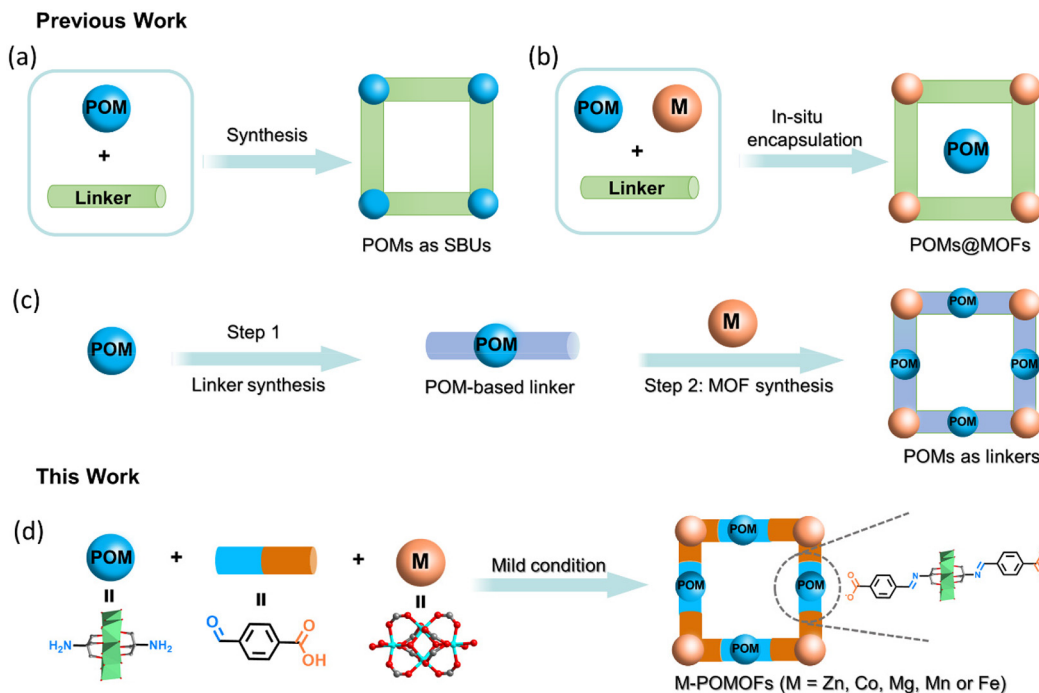
Scheme 1 Synthesis strategies of single-crystal POMOFs.

one-pot reaction, whereas method (iii) involves complicated ligand synthesis.

To address these limitations, we propose an imine bond-directed assembly of POMOFs by linking amino-functionalized Anderson-type POMs with aldehyde-terminated divalent metal clusters (Scheme 1d). This method was successfully applied to synthesize a series of isostructural M(II)-POMOFs (M = Zn, Co, Mg, or Mn). To further enhance the functions of these materials, we utilized the M(II)-POMOF as a template and applied post-synthetic metathesis-oxidation to obtain Fe(III)-POMOF. To facilitate the exchange process and preserve the overall structure, we first introduced Fe^{2+}, which has a relatively high exchange rate, forming an intermediate Fe(II)-POMOF. Subsequently, through air oxidation, we converted the Fe(II)-POMOF to the desired Fe(III)-POMOF. The simple synthetic approach avoids the harsh conditions required for the direct synthesis of POMOFs containing high-valent metals, thus maintaining the integrity of POM centers. By combining Lewis acidic Fe^{3+} and POMs, Fe(III)-POMOF showed high catalytic activity for CO_2 cycloaddition with epoxides to form cyclic carbonates.

Results and discussion

Structural design and characterization of M(II)-POMOFs

The synthetic strategy for the preparation of POM-COOH is shown in Fig. 1a. First, we grafted tris(hydroxymethyl)amino-methane (Tris) onto both sides of the Anderson POM and obtained the amino-functionalized $POM-NH_2$. Experimentally,

$POM-NH_2$ was prepared in good yield by refluxing $(TBA)_2Na_2[\alpha-Mo_8O_{26}]$, $Mn(CH_3COO)_3 \cdot 2H_2O$, and Tris in acetonitrile.[26,27] Structural analysis revealed that $POM-NH_2$ contains three TBA cations and one Tris-grafted Anderson-type cluster $[MnMo_6O_{18}(OH)_6(tris)_2]^{3-}$, which can be formulated as $(TBA)_3[MnMo_6O_{18}\{(OCH_2)_3CNH_2\}_2]$.[28] Second, M(II)-POMOFs (M = Zn, Co, Mg, or Mn) were synthesized at room temperature using $POM-NH_2$, 4-formylbenzoic acid, and metal salts as precursors in a one pot reaction. Single-crystal X-ray diffraction revealed that M(II)-POMOFs (M = Zn, Co) are isostructural (Table S1†). Taking Co-POMOF as an example, the asymmetric unit of Co-POMOF consists of two POM-based linkers, half of the $Co_4(OH)_2(COO)_6(H_2O)_6$ cluster. Each $POM-NH_2$ reacted with two 4-formylbenzoic acids through *in situ* imine condensation, forming a 2-connected linker terminated with carboxylate groups, namely POM-COOH. The carboxylate linkers were further connected to adjacent $Co_4(OH)_2(COO)_6(H_2O)_6$ clusters to self-assemble into Co-POMOF. Within the $Co_4(OH)_2(COO)_6(H_2O)_6$ cluster, four Co^{2+} ions are bridged by two μ_3-O atoms and six carboxylates. Each Co atom is in the 6-coordinated octahedral environment surrounded by oxygen atoms of the carboxylate, solvents, and μ_3-O atoms. Topologically, the $Co_4(OH)_2(COO)_6(H_2O)_6$ cluster can be regarded as a 6-connected node while POM-COOH can be simplified into a linear linker. Therefore, the overall framework can be simplified into a 3D network with a **pcu** topology (Fig. 1b). Co-POMOF has a 2-fold interpenetrated structure (Fig. 1c). The single-crystal structure of Zn-POMOF is similar to that of Co-POMOF, except that the Zn_4 clusters are three-fold disordered (Fig. S1†).
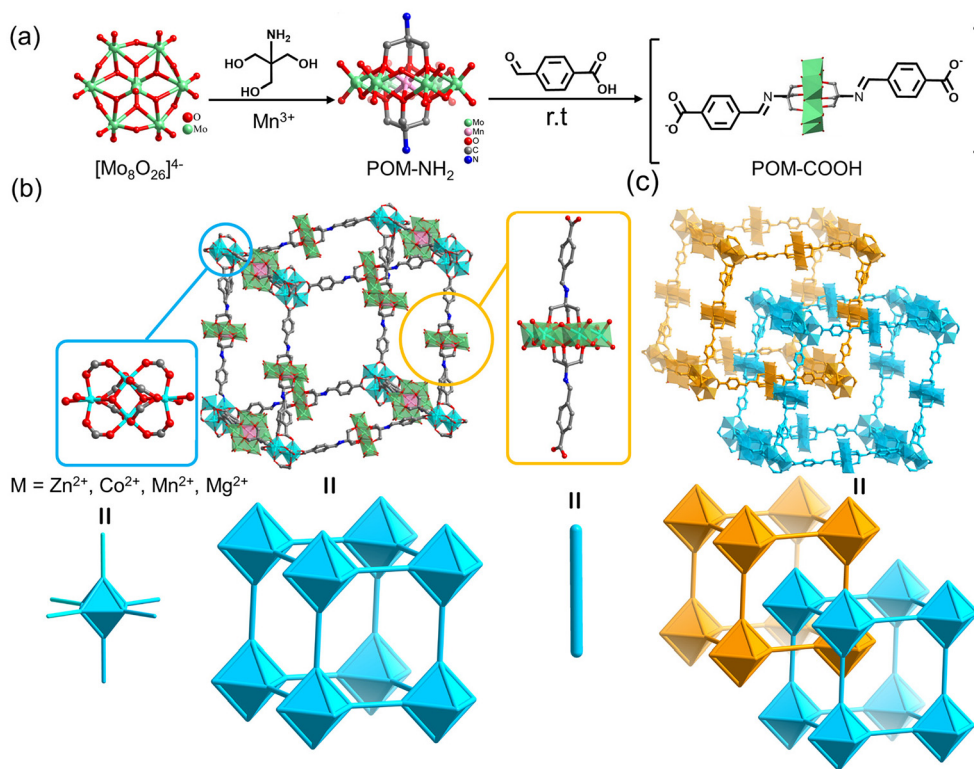
Fig. 1 (a) Synthetic route to the POM-COOH linker. The overall structure and corresponding topology of (b) Co-POMOF and (c) its 2-fold interpenetrated framework.

We propose that the imine bond directed the *in situ* assembly of POM-COOH moieties, which is important for the formation of M(II)-POMOFs. To verify our hypothesis, POM-NH$_2$ and 4-formylbenzoic acid were reacted under conditions similar to those used for the synthesis of M(II)-MOF, but without the addition of M(II), which resulted in the isolation of POM-COOH crystals (Table S1†). The single structure contains four TBA cations, two $[MnMo_6O_{18}(OH)_6(tris)_2]^{3-}$ cores, and two free carboxylic acid groups.

Similar to Zn-POMOF and Co-POMOF, microcrystals of Mn-POMOF and Mg-POMOF can be synthesized. Powder X-ray diffraction (PXRD) confirmed that M(II)-POMOFs (M = Mg, Zn, Mn, Co) are isostructural with comparable diffraction peaks. Their experimental PXRD patterns match well with simulations based on the single-crystal X-ray diffraction (SC-XRD) structure of Zn(II)-POMOF, as shown in Fig. 2a. To check the bulk purification of M-POMOF (M = Zn, Co, Mn, Mg), inductively coupled plasma optical emission spectroscopy (ICP-OES) experiments were conducted, the M (M = Zn, Co, Mg), Mn, and Mo ratio is consistent with calculations based on the molecular formula. The M(II)-POMOFs (M = Zn, Co, Mg, or Mn) and their linker fragments were characterized by Fourier transform infrared (FTIR) spectroscopy (Fig. 2b). For the M(II)-POMOFs, the peak at 907 cm^{-1} is assigned to the Mo–O vibrations of the inorganic skeleton of the POMs. The bands at 645, 555, and 780 cm^{-1} are attributed to Mo–O–Mo vibrations.[29,30] The

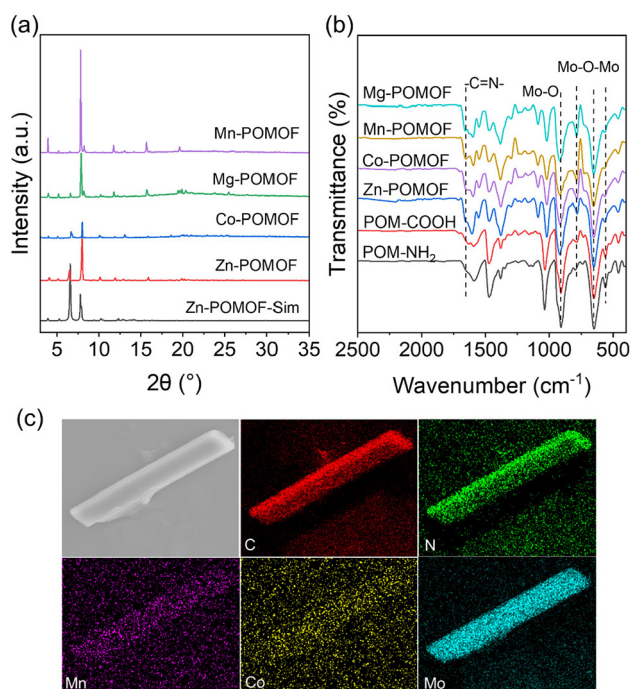

Fig. 2 (a) PXRD patterns of the as-synthesized M(II)-POMOFs (M = Zn, Co, Mg, or Mn) and simulated from the crystal structure. (b) FTIR spectrum of M-POMOFs, POM-COOH, and POM-NH$_2$. (c) SEM and mapping images of Co-POMOF.

stretching vibration of the infrared peak at 1690–1650 cm^{-1} corresponds to imine bonds.[31] Scanning electron microscopy (SEM) images of Co-POMOF and elemental mapping by energy-dispersive X-ray spectroscopy (EDS) revealed a uniform distribution of Co, Mo, and Mn elements in the MOF particles (Fig. 2c). Furthermore, as shown in Fig. S2,† thermogravimetric analysis (TGA) of the M(II)-POMOFs (M = Zn, Co, Mg, or Mn) indicated that all the materials were stable up to 250 °C. The initial mass loss observed in the TGA curve of Zn-POMOF before 100 °C is primarily due to the removal of solvent molecules. The second weight loss occurs at 250–400 °C and the corresponding mass loss is 25.1%; the weight loss in this process corresponds to the decomposition of organic linkers and, eventually, the collapse of the Zn-POMOF structure at higher temperatures. The similarity in TGA curves for Co-POMOF, Mn-POMOF, and Mg-POMOF with Zn-POMOF indicates consistent thermal behavior and solvent removal characteristics across these POMOFs, as shown in Fig. S2.†

Synthesis of Fe(III)-POMOF by metal exchange and oxidation

With the success in the synthesis of M(II)-POMOFs, we further explored the synthesis of Fe(III)-POMOF with strong Lewis acidic Fe^{3+} sites. However, direct synthesis of Fe(III)-POMOF is unsuccessful, possibly due to the harsh synthetic conditions of Fe(III)-POMOF which are incompatible with the formation of the POM-COOH linker.[32] High temperatures and excess acid modulators are usually used to synthesize Fe(III)-POMOF, which hinders the formation of labile imine bonds. Moreover, the Anderson-type POM-NH$_2$ is unstable and tends to form

Mo$_6$ during Fe(III)-POMOF synthesis.[33] Therefore, we first synthesized Zn-POMOF under acid-free conditions at room temperature and then prepared Fe(III)-POMOF through Fe^{2+} exchange and oxidation.

The metal exchange and oxidation were carried out following the literature.[34] Incubating Zn-POMOF crystals in the FeCl$_2$ solutions of anhydrous DMF under N$_2$ protection led to the formation of Fe(II)-POMOF. Exposing Fe(II)-POMOF to air resulted in the spontaneous oxidation to form Fe(III)-POMOF (Fig. 3a), which balances the charge by converting the terminal –OH$_2$ ligands into the –OH.[32] The inductively coupled plasma optical emission spectroscopy (ICP-OES) test revealed that the exchange ratio reached 95% after 12 h (Fig. 3b). The PXRD peaks are consistent with those of Zn-POMOF, which confirms that Fe(III)-POMOF has the same framework structure as the parent Zn-POMOF (Fig. 3c). The color of the crystals deepened upon metal exchange and oxidation (Fig. 3c inset), indicating the existence of Fe^{3+}. Furthermore, the transmission electron microscopy (TEM) images (Fig. 3d) revealed that Mn, Mo, and Fe were uniformly distributed in Fe(III)-POMOF particles, implying the successful metal exchange. X-ray photoelectron spectroscopy (XPS) confirms the oxidation state of Fe(III) in the Fe(III)-POMOF (Fig. S19†). The porosity of Fe(III)-POMOF was estimated using N$_2$ and CO$_2$ adsorption isotherms, which revealed low gas uptake due to the framework collapse after solvent removal (Fig. S20†). Flowing supercritical CO$_2$ was used to activate Fe(III)-POMOF, but to no avail, possibly due to the weak mechanical stability of imine-based long linkers.

Notably, Fe(III)-POMOF cannot be directly obtained through a one-pot reaction, likely due to the harsh synthetic conditions
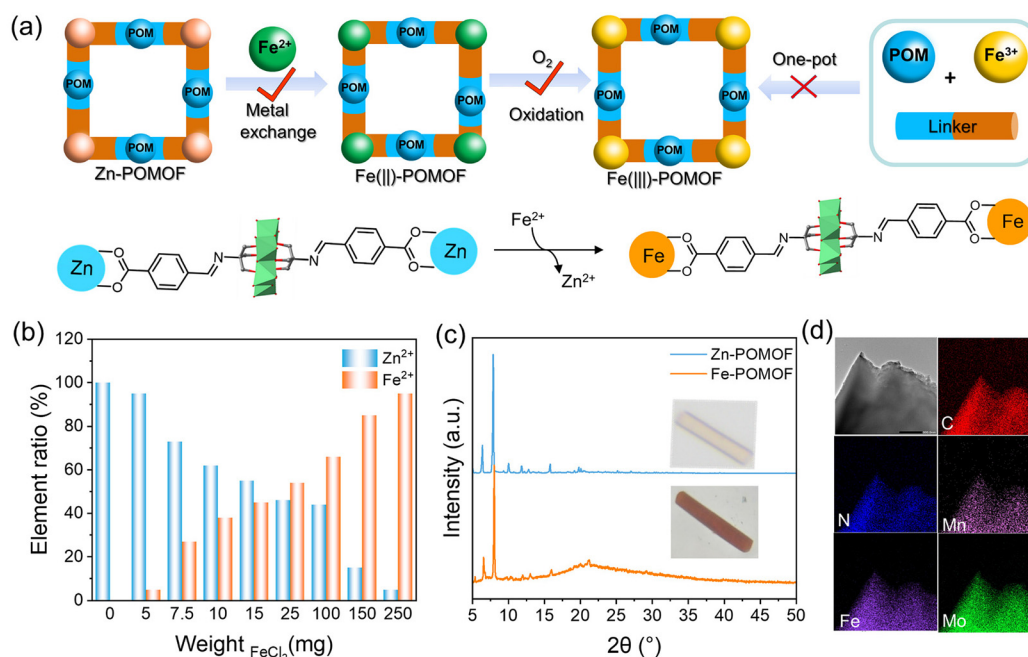

Fig. 3 (a) Formation of Fe(III)-POMOF with postsynthetic metal exchange and oxidation. (b) Elemental ratio of Zn^{2+} and Fe^{2+} in Zn–POMOF metal exchange with different amounts of FeCl$_2$. (c) PXRD patterns of the obtained Fe(III)-POMOF and pristine Zn–POMOF. (d) TEM and elemental mapping images of Fe(III)-POMOF.

required for Fe(III)-MOFs, which impede the formation of labile imine bonds. Direct synthesis of Fe(II)-POMOF from $FeCl_2$ through a one-pot method was unsuccessful possibly due to the spontaneous oxidation and hydrolysis of Fe^{2+} during MOF synthesis. Additionally, direct metal exchange using $FeCl_3$ was unsuccessful because Zn-POMOF decomposes in the solution of $FeCl_3$. These control experiments highlight the importance of metal exchange and oxidation processes in the formation of Fe(III)-POMOF. This is the first example of POMOFs containing Fe^{3+}-based SBUs to the best of our knowledge.

Catalytic cycloaddition of CO_2 with epoxides

With Lewis acidic Fe^{3+} and POMs, Fe(III)-POMOF represents a promising heterogeneous catalyst for the cycloaddition of CO_2 with epoxides to produce cyclic carbonates. CO_2 fixation with styrene oxide was carried out with a series of M(II)-POMOFs and Fe(III)-POMOF as catalysts at 50 °C under 1 atm of CO_2 in the presence of the tetrabutylammonium bromide (TBAB) cocatalyst. The yields of the cyclic carbonates were calculated by ^{1}H NMR (Fig. S3–S7†). As summarized in Table 1, diverse catalytic performances were observed, while a blank control experiment with no catalyst showed negligible product formation under identical conditions (entry 9). The conversions of the four M(II)-POMOFs were determined to be approximately 88%, 71%, 78%, and 40% for Zn, Co, Mn, and Mg-POMOF (entries 1–5 in Table 1), respectively. Interestingly, Fe(III)-POMOF exhibited much higher CO_2 fixation activity than M(II)-POMOFs, and the yield reached 98% at 48 h, which implies

that Fe played a crucial role in increasing the reaction rate. This activity trend is in line with the Lewis acidity of metal cations, where Fe(III) sites function as stronger Lewis acids.[35] To confirm the heterogeneous nature of Fe(III)-POMOF catalysts, hot filtrations were performed, and the yields remained consistent after filtering out the catalyst (Fig. S12–S18†). ICP-OES analysis of the filtrate revealed that the concentration of Fe^{3+} was 0.05 ppm, where the metal leaching was negligible during the catalytic reaction.

To study the role of Fe^{3+} and POM in catalysis, control experiments were systematically carried out by adding equal amounts of POM and $FeCl_3$. The yield was 10% in the presence of POM alone (entry 6) and 4% in the presence of only $FeCl_3$ (entry 8). To further investigate the synergistic effect between metals and POM, we mechanically mixed the metal salt $FeCl_3$ as well as the organic POM ligands in this reaction (entry 7), and the yield of the product was only 25% (Fig. S8–S10†). This low activity can be explained by the low solubility of POM, which hindered the accessibility of Lewis acidic sites. Additionally, the Fe^{3+}-based MOF, PCN-250(Fe), was tested as a control under the same conditions with a 15% yield (entry 10) (Fig. S11†). These results highlight that the high catalytic activity of the Fe(III)-POMOF framework is attributed to the synergistic effect of open iron sites and POM during the reaction.
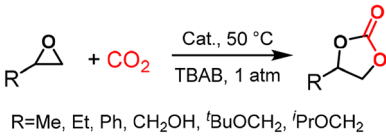
The cyclic stability and recyclability of heterogeneous catalysts are important in practical applications. The catalytic activity of Fe(III)-POMOF was well retained even after five runs (Fig. S21a and S27–31†). The PXRD results (Fig. S21b†) revealed that the crystallinity of the catalyst was maintained after the reaction, indicating the integrity of the porous framework. Considering the excellent catalytic performance of Fe(III)-POMOF, we selected several representative epoxides with different substituents under the above optimal reaction conditions to further investigate the general applicability of the catalysts. As shown in Table 1, almost all the cyclic carbonates with different substituents were obtained in high yields. The ^{1}H NMR spectra of various cycloaddition products are shown in Fig. S22–S26.†

According to the experimental process and related literature reports, a catalytic reaction mechanism was proposed.[36] The epoxide and CO_2 molecules are activated by the exposed Lewis acid sites in the MOFs. Then, the bromine anion in TBAB performs a nucleophilic attack on the α-carbon atoms in the activated epoxide, generating an intermediate alkyl carbonate anion. Meanwhile, bromoalkoxide readily undergoes nucleophilic addition reactions with polarized CO_2 molecules to form alkyl carbonates and completes the catalytic cycle.

Table 1 Cycloaddition reaction of epoxides with CO_2 under different conditions[a]

R=Me, Et, Ph, CH_2OH, $^tBuOCH_2$, $^iPrOCH_2$

Entry	R	Catalyst	Yield[b] (%)
1	Ph	Fe(III)-POMOF	98
2	Ph	Zn-POMOF	88
3	Ph	Co-POMOF	71
4	Ph	Mn-POMOF	78
5	Ph	Mg-POMOF	40
6	Ph	POM-COOH	10
7	Ph	$FeCl_3$/POM-COOH	25
8	Ph	$FeCl_3$	4
9	Ph	None[c]	n.d.
10	Ph	PCN-250	15
11	Me	Fe(III)-POMOF	98
12	Et	Fe(III)-POMOF	99
13	CH_2OH	Fe(III)-POMOF	66
14	$^tBuOCH_2$	Fe(III)-POMOF	99
15	$^iPrOCH_2$	Fe(III)-POMOF	96

[a] Reaction conditions: catalyst (0.08 mmol%, based on the M metal ion) (M = Fe(III), Zn, Co, Mn, Mg), cocatalyst TBAB (0.1 mmol), epoxide (1 mmol), CO_2 (1 atm), MeCN (2 mL), 48 h, 50 °C. [b] The yield was determined by ^{1}H NMR using CH_2Br_2 as an internal standard. [c] Without the cocatalyst or catalyst.

Conclusions

In summary, a series of isostructural M(II)-POMOFs (M = Zn, Co, Mn, Mg), which are composed of Anderson-type POMs and aldehyde-terminated divalent metal clusters in different SBUs, have been assembled under mild conditions. Additionally, an

isostructural Fe(III)-POMOF was prepared through metal exchange and oxidation strategies at room temperature. Notably, compared with M(II)-POMOFs of the same structure, Fe(III)-POMOF exhibits enhanced catalytic performance in the cyclization of CO_2 with epoxides. Our synthetic approach to realize POMOFs containing a high density of Lewis acidic catalytic centers under mild conditions is expected to facilitate the rational design and development of heterogeneous catalytic systems.

Experimental section

Syntheses of $TBA_2Na_2Mo_8O_{26}$, $POM-NH_2$

$(TBA)_3[MnMo_6O_{18}\{(OCH_2)_3CNH_2\}_2](POM-NH_2)$ and $(TBA)_2Na_2[\alpha-Mo_8O_{26}]$ were synthesized according to the literature.[23,33]

Syntheses of POM-COOH

$POM-NH_2$ (145 mg, 0.1 mmol), 4-formylbenzoic acid (30 mg, 0.2 mmol), and DMSO (1 mL) were combined in a 20 mL Pyrex vial and sonicated for 5 minutes. The resulting suspension was capped and incubated at room temperature for 24 hours to yield orange crystals. The crystals were collected by filtration and washed with fresh DMSO three times.

Synthesis of M-POMOF M(II)

$Zn(CH_3COO)_2 \cdot 2H_2O$ (50 mg, 0.23 mmol), $POM-NH_2$ (145 mg, 0.1 mmol), 4-formylbenzoic acid (30 mg, 0.2 mmol), and DMF (1 mL) were combined in a 20 mL Pyrex vial and sonicated for 5 minutes. The resulting suspension was capped and incubated at room temperature for 24 hours to yield orange crystals. The product was collected by filtration and washed with fresh DMF three times. Purple crystals of Co-POMOF, rose-red crystals of Mn-POMOF, and orange crystals of Mg-POMOF were synthesized by a similar method to that of Zn-POMOF, except that $Zn(CH_3COO)_2 \cdot 2H_2O$ was replaced by $Co(CH_3COO)_2 \cdot 2H_2O$, $Mn(CH_3COO)_2 \cdot 2H_2O$ and $Mg(CH_3COO)_2 \cdot 2H_2O$, respectively.

Synthesis of Fe(III)-POMOF

Zn-POMOF (36 mg) was incubated in the anhydrous DMF solution of $FeCl_2$ (25 mg, 1 mL) at room temperature in a glove box under N_2 protection. The supernatant was replaced for 12 h. After 12 h and exposure to air, the dark red crystals of Fe(III)-POMOF were collected by filtration and washed with fresh DMF three times (C: 22.27%, H: 2.27%, and N: 2.72% based on elemental analysis).

Catalytic reactions

The catalytic reactions were carried out in a 25 mL Schlenk flask. The catalyst (0.08 mmol%, based on the M metal ion) together with the epoxide (1 mmol) and cocatalyst of TBAB (32.5 mg, 0.1 mmol) and MeCN (2 mL) were transferred to the reactor immediately. The reactor was charged with CO_2 up to 1 atmosphere and stirred at 50 °C for 48 h. When the reaction was complete, the reactor was cooled at room temperature, and the solvent was then removed by distillation under reduced pressure. For the catalyst recycling test, the catalyst was isolated by filtration, washed several times with DMF and MeCN to fully remove the substrates, and reused in another catalytic experiment. The yield of the product was determined by ^1H NMR spectroscopy, and CH_2Br_2 was used as the internal standard.

Author contributions

All the authors contributed to the conception and design. The material preparation and catalytic reactions were performed by Xiang Yu, the analysis of catalytic results was performed by Xinyu Xu, and the crystal data collection and analysis were performed by Yi-Fan Liu, Lei Gao, and Yu-Hao Gu. TEM was performed by Rengan Luo. All the authors have read and approved the final manuscript.

Data availability

Crystallographic data for the compounds have been deposited at the Cambridge Crystallographic Data Centre (CCDC) with the accession numbers 2381572–2381575,† which can be accessed at https://www.ccdc.cam.ac.uk/. Materials, instrumentation details, synthesis procedures, and additional data including PXRD, NMR, TGA, and crystallographic tables are provided in the ESI† accompanying this article. This information is acceecssible at http://doi.org/10.1039/d4dt02609h.

Conflicts of interest

There are no conflicts to declare.

Acknowledgements

References

1 N. I. Gumerova and A. Rompel, *Nat. Rev. Chem.*, 2018, **2**, 0112.

2 B. L. Huffman, A. R. C. Bredar and J. L. Dempsey, *Nat. Rev. Chem.*, 2024, **8**, 628–643.

3 J.-M. Lin, Z.-B. Mei, C. Guo, J.-R. Li, Y. Kuang, J.-W. Shi, J.-J. Liu, X. Li, S.-L. Li, J. Liu and Y.-Q. Lan, *J. Am. Chem. Soc.*, 2024, **146**, 22797–22806.

4 D.-Y. Du, J.-S. Qin, S.-L. Li, Z.-M. Su and Y.-Q. Lan, *Chem. Soc. Rev.*, 2014, **43**, 4615–4632.

5 X. Chen, H. Wu, X. Shi and L. Wu, *Nanoscale*, 2023, **15**, 9242–9255.

6 X.-H. Liang, A.-X. Yu, X.-J. Bo, D.-Y. Du and Z.-M. Su, *Coord. Chem. Rev.*, 2023, **497**, 215427.

7 C. Zou, Z. Zhang, X. Xu, Q. Gong, J. Li and C.-D. Wu, *J. Am. Chem. Soc.*, 2011, **134**, 87–90.

8 Y. W. Liu, B. X. Wang, Q. Fu, W. Liu, Y. Wang, L. Gu, D. S. Wang and Y. D. Li, *Angew. Chem., Int. Ed.*, 2021, **60**, 22522–22528.

9 Y. Zhang, J. Liu, S. L. Li, Z. M. Su and Y. Q. Lan, *EnergyChem*, 2019, **1**, 58.

10 M.-Y. Yao, Y.-F. Liu, X.-X. Li, G.-P. Yang and S.-T. Zheng, *Chem. Commun.*, 2022, **58**, 5737–5740.

11 Q. Han, B. Qi, W. Ren, C. He, J. Niu and C. Duan, *Nat. Commun.*, 2015, **6**, 10007.

12 G. Zhai, Y. Liu, L. Lei, J. Wang, Z. Wang, Z. Zheng, P. Wang, H. Cheng, Y. Dai and B. Huang, *ACS Catal.*, 2021, **11**, 1988–1994.

13 N. Ogiwara and S. Uchida, *Chem. Catal.*, 2023, **3**, 100607.

14 D. Sloboda-Rozner, P. L. Alsters and R. Neumann, *J. Am. Chem. Soc.*, 2003, **125**, 5280–5281.

15 D. Li, Q. Xu, Y. Li, Y. Qiu, P. Ma, J. Niu and J. Wang, *Inorg. Chem.*, 2019, **58**, 4945–4953.

16 Y. Benseghir, A. Lemarchand, M. Duguet, P. Mialane, M. Gomez-Mingot, C. Roch-Marchal, T. Pino, M.-H. Ha-Thi, M. Haouas, M. Fontecave, A. Dolbecq, C. Sassoye and C. Mellot-Draznieks, *J. Am. Chem. Soc.*, 2020, **142**, 9428–9438.

17 N. Li, J. Liu, B. X. Dong and Y. Q. Lan, *Angew. Chem., Int. Ed.*, 2020, **59**, 20779–20793.

18 L. Zhang, J. Liu and Y.-Q. Lan, *Acc. Chem. Res.*, 2024, **57**, 870–883.

19 B.-B. Lu, J. Yang, Y.-Y. Liu and J.-F. Ma, *Inorg. Chem.*, 2017, **56**, 11710–11720.

20 Y.-J. Chen, X. Huang, Y. Chen, Y.-R. Wang, H. Zhang, C.-X. Li, L. Zhang, H. Zhu, R. Yang, Y.-H. Kan, S.-L. Li and Y.-Q. Lan, *CCS Chem.*, 2019, **1**, 561–570.

21 A. Ebrahimi, L. Krivosudský, A. Cherevan and D. Eder, *Coord. Chem. Rev.*, 2024, **508**, 215764.

22 S. Zhang, F. Ou, S. Ning and P. Cheng, *Inorg. Chem. Front.*, 2021, **8**, 1865–1899.

23 X. X. Li, Y. X. Wang, R. H. Wang, C. Y. Cui, C. B. Tian and G. Y. Yang, *Angew. Chem., Int. Ed.*, 2016, **55**, 6462–6466.

24 X.-X. Li, C.-C. Deng, D. Zhao, H. Yu, Q.-X. Zeng and S.-T. Zheng, *Dalton Trans.*, 2018, **47**, 16408–16412.

25 X.-X. Li, X. Ma, W.-X. Zheng, Y.-J. Qi, S.-T. Zheng and G.-Y. Yang, *Inorg. Chem.*, 2016, **55**, 8257–8259.

26 P. R. Marcoux, B. Hasenknopf, J. Vaissermann and P. Gouzerh, *Eur. J. Inorg. Chem.*, 2003, 2406–2412.

27 W. Xu, X. Pei, C. S. Diercks, H. Lyu, Z. Ji and O. M. Yaghi, *J. Am. Chem. Soc.*, 2019, **141**, 17522–17526.

28 M. P. Merkel, C. E. Anson, G. E. Kostakis and A. K. Powell, *Cryst. Growth Des.*, 2021, **21**, 3179–3190.

29 S.-Q. You, Y.-J. Dong, B.-S. Hou, M. Dong, J.-L. Tong, L.-X. Wang, X.-L. Wang, C.-Y. Sun, W. Guan and Z.-M. Su, *J. Mater. Chem. C*, 2023, **11**, 7389–7396.

30 J. Liu, N. Jiang, J. M. Lin, Z. B. Mei, L. Z. Dong, Y. Kuang, J. J. Liu, S. J. Yao, S. L. Li and Y. Q. Lan, *Angew. Chem., Int. Ed.*, 2023, **62**, e202304728.

31 L. Grunenberg, G. Savasci, M. W. Terban, V. Duppel, I. Moudrakovski, M. Etter, R. E. Dinnebier, C. Ochsenfeld and B. V. Lotsch, *J. Am. Chem. Soc.*, 2021, **143**, 3430–3438.

32 T.-F. Liu, L. Zou, D. Feng, Y.-P. Chen, S. Fordham, X. Wang, Y. Liu and H.-C. Zhou, *J. Am. Chem. Soc.*, 2014, **136**, 7813–7816.

33 W. Deng, Q. Zhang and Y. Wang, *Dalton Trans.*, 2012, **41**, 10071.

34 Y. Han, M. A. Sinnwell, R. G. Surbella, W. Xue, H. Huang, J. Zheng, B. Peng, G. Verma, Y. Yang, L. Liu, S. Ma and P. K. Thallapally, *Chem. Mater.*, 2020, **32**, 5192–5199.

35 M. Loipersberger, D. G. A. Cabral, D. B. K. Chu and M. Head-Gordon, *J. Am. Chem. Soc.*, 2021, **143**, 744–763.

36 Z. Fang, Z. Deng, X. Y. Wan, Z. Y. Li, X. Ma, S. Hussain, Z. Z. Ye and X. S. Peng, *Appl. Catal., B*, 2021, **296**, 120329.